Cite as: S. Patra *et al.*, *Science* 10.1126/science.aba0453 (2020).

Proton-electron mass ratio from laser spectroscopy of HD^+ at the part-per-trillion level

Sayan Patra[1], M. Germann[1]*, J.-Ph. Karr[2,3], M. Haidar[2], L. Hilico[2,3], V. I. Korobov[4], F. M. J. Cozijn[1], K. S. E. Eikema[1,5], W. Ubachs[1,5], J. C. J. Koelemeij[1]†

[1]LaserLaB, Department of Physics and Astronomy, Vrije Universiteit Amsterdam, De Boelelaan 1081, 1081 HV Amsterdam, Netherlands. [2]Laboratoire Kastler Brossel, UPMC-Sorbonne Université, CNRS, ENS-PSL Research University, Collège de France, 4 place Jussieu, 75005 Paris, France. [3]Université d'Evry-Val d'Essonne, Université Paris-Saclay, Boulevard François Mitterrand, 91000 Evry, France. [4]Bogolyubov Laboratory of Theoretical Physics, Joint Institute for Nuclear Research, Dubna 141980, Russia. [5]ARCNL (Advanced Research Centre for Nanolithography), Science Park 106, 1098 XG Amsterdam, Netherlands.

*Present address: Department of Physics, Umeå University, 901 87 Umeå, Sweden.

†Corresponding author. Email: j.c.j.koelemeij@vu.nl

Recent mass measurements of light atomic nuclei in Penning traps have indicated possible inconsistencies in closely related physical constants like the proton-electron and deuteron-proton mass ratios. These quantities also influence the predicted vibrational spectrum of the deuterated molecular hydrogen ion in its electronic ground state. We measure the frequency of the $\nu = 0 \rightarrow 9$ overtone transition of this spectrum with an uncertainty of 2.9 parts-per-trillion through Doppler-free two-photon laser spectroscopy. Leveraging high-precision ab initio calculations we convert our measurement to tight constraints on the proton-electron and deuteron-proton mass ratios, consistent with the most recent Penning-trap determinations of these quantities. This results in an unprecedented precision of 21 parts-per-trillion for the value of the proton-electron mass ratio.

Precision measurements on simple atomic systems and their constituents play an essential role in the determination of physical constants. Examples range from the proton-electron mass ratio, m_p/m_e, whose value depends strongly on measurements performed on single protons and hydrogen-like ions stored in Penning traps, to the Rydberg constant, R_∞, and proton electric charge radius, r_p, which are derived from spectroscopic measurements of energy intervals in atomic hydrogen-like systems (*1*, *2*). It is desirable to perform such determinations of physical constants redundantly using different systems and methods, as this provides a crucial cross-check for possible experimental inconsistencies or new physical effects beyond our current understanding of nature. This is illustrated by the "Proton Radius Puzzle," a 5.6σ discrepancy between the value of r_p obtained from muonic-hydrogen spectroscopy and the 2014 Committee on Data for Science and Technology (CODATA-2014) reference value (*1*, *3*). Progress toward solution of the puzzle was made after most of the recent r_p determinations from electron-proton scattering and atomic-hydrogen spectroscopy were found to be consistent with the muonic-hydrogen value (*4*–*7*). A similar need for alternative measurements is indicated for m_p/m_e – an important dimensionless quantity which sets the scale of rotations and vibrations in molecules – since recent Penning-trap measurements of the relative atomic masses of light atomic nuclei (including those of the proton, m_p, deuteron, m_d, and helion, m_h) differed by several standard deviations from earlier results (*8*–*15*). For example, Ref. (*11*) determined m_p with 32 parts-per-trillion (ppt) precision, three times higher than the then-accepted CODATA-2014 value, but also found it to be smaller by 3σ (*11*, *12*). The value from (*11*) has been incorporated in the 2017 and forthcoming 2018 CODATA adjustments, but uncertainty margins were increased by a factor of 1.7 to accommodate the difference (*2*). This currently limits the precision of m_p/m_e (obtained by dividing m_p by the more precise CODATA-2018 value of m_e) to 60 ppt. This in turn diminishes the predictive power of ab initio calculations of rotational-vibrational spectra of molecular hydrogen ions (H_2^+, HD^+) and antiprotonic helium, which have achieved a precision of 7-8 ppt (*16*).

The high theoretical precision in principle enables an improved determination of m_p/m_e from spectroscopy of molecular hydrogen ions, which could shed light on this situation (*17*). However, this requires measurements with ppt-level uncertainties, two orders of magnitude beyond state-of-the-art laser (*18*, *19*) and terahertz (*20*) spectroscopy of HD^+ and antiprotonic helium. Here, we present a frequency measurement of the (v,L): $(0,3) \rightarrow (9,3)$ vibrational transition in the electronic ground state of HD^+ with 2.9 ppt uncertainty, significantly more precise than the theoretical uncertainty. This allows us to extract a new value of m_p/m_e with unprecedented precision, while providing a cross-link to other physical constants, which enables additional consistency checks of their values.

We previously identified the (v,L): (0,3) → (4,2) → (9,3) two-photon transition in HD^+ (Fig. 1A) as a promising candidate for high-resolution Doppler-free laser spectroscopy (*21*), owing to the near degeneracy of the 1442 nm and 1445 nm photons involved, and the possibility to store HD^+ ions in a linear Paul trap while cooling them to 10 mK through Coulomb interaction with co-trapped beryllium ions, themselves cooled by 313 nm laser radiation. We showed that for counter-propagating 1442 nm and 1445 nm laser beams directed along the trap's symmetry axis, Doppler-free vibrational excitation of HD^+ deep in the optical Lamb-Dicke regime may be achieved. Thus, with a natural linewidth of 13 Hz, Q-factors of $>10^{13}$ come within reach. We use phase-stabilized, continuous-wave external cavity diode lasers at 1442 nm and 1445 nm possessing line widths of 1–2 kHz to vibrationally excite cold, trapped HD^+ ions (*22*). Optical frequencies are measured with an uncertainty below 1 ppt using an optical frequency comb laser, while two-photon excitation is detected through enhanced loss of HD^+ from the trap owing to state-selective dissociation of molecules in the $v = 9$ state by 532 nm laser radiation (*22*, *23*).

Rovibrational energy levels of HD^+ exhibit hyperfine structure caused by magnetic interactions between the spins of the proton, $\mathbf{I}_p$, deuteron, $\mathbf{I}_d$, and electron, $\mathbf{s}_e$, as well as the molecule's rotational angular momentum, $\mathbf{L}$ (*24*). The spins are coupled to form resultant angular momenta $\mathbf{F} = \mathbf{s}_e + \mathbf{I}_p$ and $\mathbf{S} = \mathbf{F} + \mathbf{I}_d$, and are finally coupled with $\mathbf{L}$ to form the total angular momentum $\mathbf{J} = \mathbf{S} + \mathbf{L}$. Here, we observe transitions $(v,L; F,S,J)$: (0,3;1,2,5) → (9,3;1,2,5) (henceforth referred to as the "$F = 1$ transition"), and $(v,L; F,S,J)$: (0,3;0,1,4) → (9,3;0,1,4) (referred to as the "$F = 0$ transition"); see Fig. 1B.

To record a spectrum, we keep the 1442 nm laser frequency, ν_F (with $F = 0,1$; see Fig. 1B), at a fixed detuning δ_F from resonance to avoid excessive population of the intermediate v=4 state (*21*, *22*). Meanwhile, we step the 1445 nm laser frequency, ν'_F, in intervals of 2 kHz over the range of interest (Fig. 1B). At each step we let all lasers interact with the HD^+ ions for 30 s, after which we determine the cumulative loss of HD^+, and add the resulting data point to the spectrum (*22*). A typical spectrum covers a span of 40 to 60 kHz with on average nine points per frequency, and with the 180 to 270 data points acquired in random order over the course of about ten measurement days. The signal-to-noise ratio of the $F = 0$ spectrum turned out to be lower than its $F = 1$ counterpart, which we attribute to smaller available population in the initial state, and slower re-population by blackbody radiation (*21*). To increase the $F = 0$ signal, we apply two radio-frequency (rf) magnetic fields driving population from the (F,S,J) = (1,2,5) and (1,2,4) states of the $v = 0$, $L = 3$ hyperfine manifold to the (F,S,J) = (0,1,4) states; see Fig. 1B and fig. S1 (*22*). Recorded spectra of the $F = 0$ and $F = 1$ transitions are shown in Fig. 2.

The interpretation of the recorded spectra requires an analysis of several systematic effects which affect the line shape and position (*22*). Here we exploit the good theoretical accessibility of the HD^+ molecule (*25*), which allows a priori estimation of these effects. Zeeman and Stark effects are calculated to shift the $F = 0$ and $F = 1$ lines by up to 0.5 kHz, which occurs through level shifting as well as line shape deformation (*22*). Expected two-photon power broadening and interaction-time broadening stemming from the 9×10^3 s^{-1} rate of dissociation of molecules in the $v = 9$ state (*21*) satisfactorily explain the observed line widths of 8(3) kHz. In addition, we experimentally investigated a number of systematic effects, yielding results consistent with the theory-based estimates (*22*). The size and uncertainty of leading systematic effects are listed in Table 1.

As shown in Fig. 2, Lorentzian line shapes are fitted to the spectra to find their respective line centers with 0.6–0.7 kHz uncertainty. These are subsequently corrected for systematic frequency shifts, and combined to arrive at the $F = 0$ and $F = 1$ transition frequencies, $\nu_{HF0,exp}$, and $\nu_{HF1,exp}$ (*22*); see Fig. 2, C and D, and Table 2. These frequencies are related to the spin-averaged (i.e., pure rovibrational) frequency, ν_{SA}, through the relations $\nu_{SA} = \nu_{HF0} - f_{0c}$ and $\nu_{SA} = \nu_{HF1} - f_{1c}$ (Fig. 1C). Because only ν_{SA} depends directly on the values of the physical constants of interest, we need to determine and correct for the hyperfine shifts, $f_{1c} \approx -63$ MHz and $f_{0c} \approx 115$ MHz to derive ν_{SA}. We take the hyperfine intervals, $f_{0c,theo}$ and $f_{1c,theo}$ from theory (*22*, *24*, *26*), and compute $\nu_{SA,exp}$ as the mean of $\nu_{HF0,exp} - f_{0c,theo}$ and $\nu_{HF1,exp} - f_{1c,theo}$ (*22*). In this process, we expand the uncertainties of the theoretical hyperfine intervals by about a factor of two (*22*), so that the theoretical hyperfine interval, $f_{10,theo}$, becomes consistent with its measured counterpart, $f_{10,exp} \equiv \nu_{HF0,exp} - \nu_{HF1,exp}$ (Table 2). We thus find $\nu_{SA,exp}$ = 415,264,925,500.5(0.4)$_{exp}$(1.1)$_{theo}$(1.2)$_{total}$ kHz.

Our experimental frequency $\nu_{SA,exp}$ exceeds the theoretical frequency $\nu_{SA,theo}$ (CODATA-2014) = 415,264,925,467.1(10.2) kHz by 33.4 kHz, or 3.3σ, when we use CODATA-2014 physical constants to compute $\nu_{SA,theo}$ (*22*, *27*). The uncertainties of these constants dominate the 10.2 kHz uncertainty rather than the 3.1 kHz precision of the theoretical model; m_p/m_e for example contributes 9.0 kHz (fig. S3) (*22*). Using known sensitivity coefficients (*17*, *22*), we can also compute other theoretical frequency values, $\nu_{SA,theo}$ (k), for other combinations (labeled k) of values of physical constants. For example, a more precise value is obtained by use of CODATA-2018 constants, $\nu_{SA,theo}$ (CODATA-2018) = 415,264,925,496.2(7.4) kHz. This state-of-the-art value is shifted by 29.1 kHz with respect to the CODATA-2014 value (Fig. 3A), and essentially closes the 33.4 kHz gap with our experimental value $\nu_{SA,exp}$. Figure 3A furthermore shows that most of the 29.1 kHz shift stems from the smaller CODATA-2018 value of m_p/m_e. A smaller part, 5.1 kHz, is due to the CODATA-2018 updated values of

r_p, r_d, and R_∞, which are essentially equal to the muonic-hydrogen values (*3*, *28*). The 5.1 kHz shift, which is four times larger than our experimental uncertainty and comparable to the current theoretical precision, therefore reveals the impact of the Proton Radius Puzzle on molecular vibrations. We obtain even better precision (5.5 kHz) and agreement after replacing the CODATA-2018 value of m_p/m_e with that from (*11*, *12*), this time leading to a 31.2 kHz shift (Fig. 3A).

We may also invert the procedure and derive a new value of m_p/m_e from the difference $\nu_{SA,exp} - \nu_{SA,theo}$ (*k*); see Fig. 3B. Using $\nu_{SA,theo}$ (CODATA-2018), we obtain m_p/m_e (HD^+) = 1,836.152 673 349(71) which is slightly more precise than, and in excellent agreement with, the value of m_p/m_e from (*12*). With $\nu_{SA,theo}$ being also sensitive to the deuteron-proton mass ratio (*22*), one may alternatively extract a two-dimensional constraint in the (m_p/m_e, m_d/m_p) plane (Fig. 3C). Our result is found to be in good agreement with both m_p/m_e from (*12*) and the recent value of m_d/m_p (*14*), assuming CODATA-2018 values of r_p, r_d, and R_∞. This justifies a determination of m_p/m_e from all three results shown in Fig. 3C combined, leading to a value of 1,836.152 673 406(38) (bottommost point in Fig. 3B) which, at 21 ppt precision, represents the most precise determination of this quantity to date. The data shown in Fig. 3C can furthermore be combined with the CODATA-2018 value of m_e and the value of m_h from (*15*) to obtain the atomic mass difference $m_p + m_d - m_h$ = 0.005 897 432 54(12) u. The same quantity has previously been determined from the measured mass ratio $^3He^+/HD^+$ (*13*), leading to $m_p + m_d - m_h$ = 0.005 897 432 19(7) u. The two results differ by 0.35(14) nu, or 2.5σ. We thereby confirm the "^{3}He puzzle," a term used to describe similar deviations of 0.48(10) nu (or 4.8σ) and 0.33(13) nu (or 2.4σ) reported earlier in (*13*) and (*14*), respectively.

Our work establishes precision spectroscopy of HD^+, combined with ab initio quantum-molecular calculations, as a state-of-the-art method for determining fundamental mass ratios. It furthermore provides a link between mass ratios and other physical constants, such as R_∞, and sheds light on the large deviations seen between recent determinations of their values. We anticipate that our results will have a notable impact on the consistency and precision of future reference values of physical constants, and enhance the predictive power of ab initio calculations of physical quantities.

REFERENCES AND NOTES

1. P. J. Mohr, D. B. Newell, B. N. Taylor, CODATA Recommended Values of the Fundamental Physical Constants: 2014. *J. Phys. Chem. Ref. Data* **45**, 043102 (2016). doi:10.1063/1.4954402
2. P. J. Mohr, D. B. Newell, B. N. Taylor, E. Tiesinga, Data and analysis for the CODATA 2017 special fundamental constants adjustment. *Metrologia* **55**, 125–146 (2018). doi:10.1088/1681-7575/aa99bc
3. A. Antognini, F. Nez, K. Schuhmann, F. D. Amaro, F. Biraben, J. M. R. Cardoso, D. S. Covita, A. Dax, S. Dhawan, M. Diepold, L. M. P. Fernandes, A. Giesen, A. L. Gouvea, T. Graf, T. W. Hänsch, P. Indelicato, L. Julien, C.-Y. Kao, P. Knowles, F. Kottmann, E.-O. Le Bigot, Y.-W. Liu, J. A. M. Lopes, L. Ludhova, C. M. B. Monteiro, F. Mulhauser, T. Nebel, P. Rabinowitz, J. M. F. dos Santos, L. A. Schaller, C. Schwob, D. Taqqu, J. F. C. A. Veloso, J. Vogelsang, R. Pohl, Proton structure from the measurement of 2S-2P transition frequencies of muonic hydrogen. *Science* **339**, 417–420 (2013). doi:10.1126/science.1230016 Medline
4. A. Beyer, L. Maisenbacher, A. Matveev, R. Pohl, K. Khabarova, A. Grinin, T. Lamour, D. C. Yost, T. W. Hänsch, N. Kolachevsky, T. Udem, The Rydberg constant and proton size from atomic hydrogen. *Science* **358**, 79–85 (2017). doi:10.1126/science.aah6677 Medline
5. H. Fleurbaey, S. Galtier, S. Thomas, M. Bonnaud, L. Julien, F. Biraben, F. Nez, M. Abgrall, J. Guéna, New measurement of the 1*S*–3*S* transition frequency of hydrogen: Contribution to the proton charge radius puzzle. *Phys. Rev. Lett.* **120**, 183001 (2018). doi:10.1103/PhysRevLett.120.183001 Medline
6. N. Bezginov, T. Valdez, M. Horbatsch, A. Marsman, A. C. Vutha, E. A. Hessels, A measurement of the atomic hydrogen Lamb shift and the proton charge radius. *Science* **365**, 1007–1012 (2019). doi:10.1126/science.aau7807 Medline
7. W. Xiong, A. Gasparian, H. Gao, D. Dutta, M. Khandaker, N. Liyanage, E. Pasyuk, C. Peng, X. Bai, L. Ye, K. Gnanvo, C. Gu, M. Levillain, X. Yan, D. W. Higinbotham, M. Meziane, Z. Ye, K. Adhikari, B. Aljawrneh, H. Bhatt, D. Bhetuwal, J. Brock, V. Burkert, C. Carlin, A. Deur, D. Di, J. Dunne, P. Ekanayaka, L. El-Fassi, B. Emmich, L. Gan, O. Glamazdin, M. L. Kabir, A. Karki, C. Keith, S. Kowalski, V. Lagerquist, I. Larin, T. Liu, A. Liyanage, J. Maxwell, D. Meekins, S. J. Nazeer, V. Nelyubin, H. Nguyen, R. Pedroni, C. Perdrisat, J. Pierce, V. Punjabi, M. Shabestari, A. Shahinyan, R. Silwal, S. Stepanyan, A. Subedi, V. V. Tarasov, N. Ton, Y. Zhang, Z. W. Zhao, A small proton charge radius from an electron-proton scattering experiment. *Nature* **575**, 147–150 (2019). doi:10.1038/s41586-019-1721-2 Medline
8. R. S. Van Dyck Jr., D. L. Farnham, S. L. Zafonte, P. B. Schwinberg, High precision Penning trap mass spectroscopy and a new measurement of the proton's "atomic mass.". *AIP Conf. Proc.* **457**, 101–110 (1999). doi:10.1063/1.57450
9. I. Bergström, T. Fritioff, R. Schuch, J. Schönfelder, On the masses of ^{28}Si and the proton determined in a Penning trap. *Phys. Scr.* **66**, 201–207 (2002). doi:10.1238/Physica.Regular.066a00201
10. A. Solders, I. Bergström, S. Nagy, M. Suhonen, R. Schuch, Determination of the proton mass from a measurement of the cyclotron frequencies of D^+ and H_2^+ in a Penning trap. *Phys. Rev. A* **78**, 012514 (2008). doi:10.1103/PhysRevA.78.012514
11. F. Heiße, F. Köhler-Langes, S. Rau, J. Hou, S. Junck, A. Kracke, A. Mooser, W. Quint, S. Ulmer, G. Werth, K. Blaum, S. Sturm, High-precision measurement of the proton's atomic mass. *Phys. Rev. Lett.* **119**, 033001 (2017). doi:10.1103/PhysRevLett.119.033001 Medline
12. F. Heiße, S. Rau, F. Köhler-Langes, W. Quint, G. Werth, S. Sturm, K. Blaum, High-precision mass spectrometer for light ions. *Phys. Rev. A* **100**, 022518 (2019). doi:10.1103/PhysRevA.100.022518
13. S. Hamzeloui, J. A. Smith, D. J. Fink, E. G. Myers, Precision mass ratio of $^3He^+$ to HD^+. *Phys. Rev. A* **96**, 060501(R) (2017). doi:10.1103/PhysRevA.96.060501
14. D. J. Fink, E. G. Myers, Deuteron-to-proton mass ratio from the cyclotron frequency ratio of H_2^+ to D^+ with H_2^+ in a resolved vibrational state. *Phys. Rev. Lett.* **124**, 013001 (2020). doi:10.1103/PhysRevLett.124.013001 Medline
15. S. L. Zafonte, R. S. Van Dyck Jr., Ultra-precise single-ion atomic mass measurements on deuterium and helium-3. *Metrologia* **52**, 280–290 (2015). doi:10.1088/0026-1394/52/2/280
16. V. I. Korobov, L. Hilico, J.-Ph. Karr, Fundamental transitions and ionization energies of the hydrogen molecular ions with few ppt uncertainty. *Phys. Rev. Lett.* **118**, 233001 (2017). doi:10.1103/PhysRevLett.118.233001 Medline
17. J.-Ph. Karr, L. Hilico, J. C. J. Koelemeij, V. I. Korobov, Hydrogen molecular ions for improved determination of fundamental constants. *Phys. Rev. A* **94**, 050501(R) (2016). doi:10.1103/PhysRevA.94.050501
18. J. Biesheuvel, J.-Ph. Karr, L. Hilico, K. S. E. Eikema, W. Ubachs, J. C. J. Koelemeij, Probing QED and fundamental constants through laser spectroscopy of vibrational transitions in HD^+. *Nat. Commun.* **7**, 10385 (2016). doi:10.1038/ncomms10385 Medline
19. M. Hori, H. Aghai-Khozani, A. Sótér, D. Barna, A. Dax, R. Hayano, T. Kobayashi, Y. Murakami, K. Todoroki, H. Yamada, D. Horváth, L. Venturelli, Buffer-gas cooling of antiprotonic helium to 1.5 to 1.7 K, and antiproton-to-electron mass ratio. *Science* **354**, 610–614 (2016). doi:10.1126/science.aaf6702 Medline
20. S. Alighanbari, M. Hansen, V. I. Korobov, S. Schiller, Rotational spectroscopy of

cold and trapped molecular ions in the Lamb-Dicke regime. *Nat. Phys.* **14**, 555–559 (2018). doi:10.1038/s41567-018-0074-3
21. V. Q. Tran, J.-Ph. Karr, A. Douillet, J. C. J. Koelemeij, L. Hilico, Two-photon spectroscopy of trapped HD^+ ions in the Lamb-Dicke regime. *Phys. Rev. A* **88**, 033421 (2013). doi:10.1103/PhysRevA.88.033421
22. Materials and methods are available as supplementary materials at the *Science* website.
23. J. Biesheuvel, J.-Ph. Karr, L. Hilico, K. S. E. Eikema, W. Ubachs, J. C. J. Koelemeij, High-precision spectroscopy of the HD^+ molecule at the 1-p.p.b. level. *Appl. Phys. B* **123**, 23 (2017). doi:10.1007/s00340-016-6576-8
24. D. Bakalov, V. I. Korobov, S. Schiller, High-precision calculation of the hyperfine structure of the HD^+ ion. *Phys. Rev. Lett.* **97**, 243001 (2006). doi:10.1103/PhysRevLett.97.243001 Medline
25. J.-Ph. Karr, H_2^+ and HD^+: Candidates for a molecular clock. *J. Mol. Spectrosc.* **300**, 37–43 (2014). doi:10.1016/j.jms.2014.03.016
26. V. I. Korobov, J. C. J. Koelemeij, L. Hilico, J.-Ph. Karr, Theoretical hyperfine structure of the molecular hydrogen ion at the 1 ppm level. *Phys. Rev. Lett.* **116**, 053003 (2016). doi:10.1103/PhysRevLett.116.053003 Medline
27. D. T. Aznabayev, A. K. Bekbaev, V. I. Korobov, Leading-order relativistic corrections to the rovibrational spectrum of H_2^+ and HD^+ molecular ions. *Phys. Rev. A* **99**, 012501 (2019). doi:10.1103/PhysRevA.99.012501
28. R. Pohl, F. Nez, L. M. P. Fernandes, F. D. Amaro, F. Biraben, J. M. R. Cardoso, D. S. Covita, A. Dax, S. Dhawan, M. Diepold, A. Giesen, A. L. Gouvea, T. Graf, T. W. Hänsch, P. Indelicato, L. Julien, P. Knowles, F. Kottmann, E.-O. Le Bigot, Y.-W. Liu, J. A. M. Lopes, L. Ludhova, C. M. B. Monteiro, F. Mulhauser, T. Nebel, P. Rabinowitz, J. M. F. dos Santos, L. A. Schaller, K. Schuhmann, C. Schwob, D. Taqqu, J. F. C. A. Veloso, A. Antognini; CREMA Collaboration, Laser spectroscopy of muonic deuterium. *Science* **353**, 669–673 (2016). doi:10.1126/science.aaf2468 Medline
29. J. C. J. Koelemeij, D. W. E. Noom, D. de Jong, M. A. Haddad, W. Ubachs, Observation of the $v'=8 \leftarrow v=0$ vibrational overtone in cold trapped HD^+. *Appl. Phys. B* **107**, 1075–1085 (2012). doi:10.1007/s00340-011-4802-y
30. H. Telle, B. Lipphardt, J. Stenger, Kerr-lens, mode-locked lasers as transfer oscillators for optical frequency measurements. *Appl. Phys. B* **74**, 1–6 (2002). doi:10.1007/s003400100735
31. M. Douglas, N. M. Kroll, Quantum electrodynamical corrections to the fine structure of helium. *Ann. Phys.* **82**, 89–155 (1974). doi:10.1016/0003-4916(74)90333-9
32. K. Pachucki, Quantum electrodynamics effects on helium fine structure. *J. Phys. B* **32**, 137–152 (1999). doi:10.1088/0953-4075/32/1/014
33. M. Haidar, Z.-X. Zhong, V. I. Korobov, J.-Ph. Karr, Nonrelativistic QED approach to the fine- and hyperfine-structure corrections of order $m\alpha^6$ and $m\alpha^6$ (m/M): Application to the hydrogen atom. *Phys. Rev. A* **101**, 022501 (2020). doi:10.1103/PhysRevA.101.022501
34. D. Bakalov, V. I. Korobov, S. Schiller, Magnetic field effects in the transitions of the HD^+ molecular ion and precision spectroscopy. *J. Phys. B* **44**, 025003 (2011). doi:10.1088/0953-4075/44/2/025003
35. S. Schiller, D. Bakalov, A. K. Bekbaev, V. I. Korobov, Static and dynamic polarizability and the Stark and blackbody-radiation frequency shifts of the molecular hydrogen ions H_2^+, HD^+, and $D2^+$. *Phys. Rev. A* **89**, 052521 (2014). doi:10.1103/PhysRevA.89.052521
36. W. Happer, B. S. Mathur, Effective operator formalism in optical pumping. *Phys. Rev.* **163**, 12–25 (1967). doi:10.1103/PhysRev.163.12
37. J. C. J. Koelemeij, Infrared dynamic polarizability of HD^+ rovibrational states. *Phys. Chem. Chem. Phys.* **13**, 18844–18851 (2011). doi:10.1039/c1cp21204d Medline
38. D. Bakalov, S. Schiller, The electric quadrupole moment of molecular hydrogen ions and their potential for a molecular ion clock. *Appl. Phys. B* **114**, 213–230 (2014). doi:10.1007/s00340-013-5703-z
39. D. Bakalov, S. Schiller, Erratum to: The electric quadrupole moment of molecular hydrogen ions and their potential for a molecular ion clock. *Appl. Phys. B* **116**, 777–778 (2014). doi:10.1007/s00340-014-5902-2
40. S. Patra, Ph.D. dissertation, Vrije Universiteit Amsterdam (2019).
41. F. Low, Natural line shape. *Phys. Rev.* **88**, 53–57 (1952). doi:10.1103/PhysRev.88.53
42. T. Udem, L. Maisenbacher, A. Matveev, V. Andreev, A. Grinin, A. Beyer, N. Kolachevsky, R. Pohl, D. C. Yost, T. W. Hänsch, Quantum Interference Line Shifts of Broad Dipole-Allowed Transitions. *Ann. Phys.* **531**, 1900044 (2019). doi:10.1002/andp.201900044
43. https://physics.nist.gov/cuu/Constants/index.html
44. S. Patra, J.-Ph. Karr, L. Hilico, M. Germann, V. I. Korobov, J. C. J. Koelemeij, Proton–electron mass ratio from HD^+ revisited. *J. Phys. B* **51**, 024003 (2018). doi:10.1088/1361-6455/aa9b92
45. P. J. Mohr, B. N. Taylor, CODATA recommended values of the fundamental physical constants: 1998. *Rev. Mod. Phys.* **72**, 351–495 (2000). doi:10.1103/RevModPhys.72.351
46. C. G. Parthey, A. Matveev, J. Alnis, B. Bernhardt, A. Beyer, R. Holzwarth, A. Maistrou, R. Pohl, K. Predehl, T. Udem, T. Wilken, N. Kolachevsky, M. Abgrall, D. Rovera, C. Salomon, P. Laurent, T. W. Hänsch, Improved measurement of the hydrogen 1*S*-2*S* transition frequency. *Phys. Rev. Lett.* **107**, 203001 (2011). doi:10.1103/PhysRevLett.107.203001 Medline
47. K. Pachucki, V. Patkóš, V. A. Yerokhin, Three-photon-exchange nuclear structure correction in hydrogenic systems. *Phys. Rev. A* **97**, 062511 (2018). doi:10.1103/PhysRevA.97.062511

ACKNOWLEDGMENTS

We are indebted to Rob Kortekaas, Tjeerd Pinkert, and the Electronic Engineering Group of the Faculty of Science at Vrije Universiteit Amsterdam for technical assistance. **Funding:** We acknowledge support from the Netherlands Organisation for Scientific Research (FOM Programs "Broken Mirrors & Drifting Constants" and "The Mysterious Size of the Proton"; FOM 13PR3109, STW Vidi 12346), the European Research Council (AdG 670168 Ubachs, AdG 695677 Eikema), the COST Action CA17113 TIPICQA, and the Dutch-French bilateral Van Gogh program. J.-Ph. K. acknowledges support as a fellow of the Institut Universitaire de France. VIK acknowledges support of the Russian Foundation for Basic Research under Grant No.~19-02-00058-a. **Author contributions:** J.C.J.K. conceived the experiment; S.P., M.G., F.M.J.C., W.U., K.S.E.E., J.C.J.K., J.-Ph.K., and L.H. designed the experiment; J.-Ph.K., M.H., and V.I.K. developed the theory and performed numerical calculations; S.P., M.G., J.-Ph.K., M.H., L.H., and J.C.J.K. set up and performed numerical simulations for analysis of systematic effects; S.P., M.G., F.M.J.C., K.S.E.E. and J.C.J.K. built the experiment; S.P. and M.G. performed the measurements; S.P., M.G., and J.C.J.K. analyzed the data; S.P., M.G., and J.C.J.K. wrote the manuscript with input from all other authors; and J.-Ph.K., L.H., K.S.E.E., W.U., and J.C.J.K. planned and supervised the project. **Competing interests:** One of the authors (JCJK) is co-founder and shareholder of OPNT bv. Authors declare no further competing interests. **Data and materials availability:** Computer code and experimental data used to obtain the results of the main text and supplementary materials are available from S. Patra *et al*., Data for: proton-electron mass ratio from laser spectroscopy of HD^+ at the part-per-trillion level, DataverseNL (2020); https://hdl.handle.net/10411/QCCLF3.

SUPPLEMENTARY MATERIALS

science.sciencemag.org/cgi/content/full/science.aba0453/DC1
Materials and Methods
Figs. S1 to S3
Tables S1 to S3
References (*29*–*47*)

5 November 2019; accepted 17 July 2020
Published online 30 July 2020
10.1126/science.aba0453

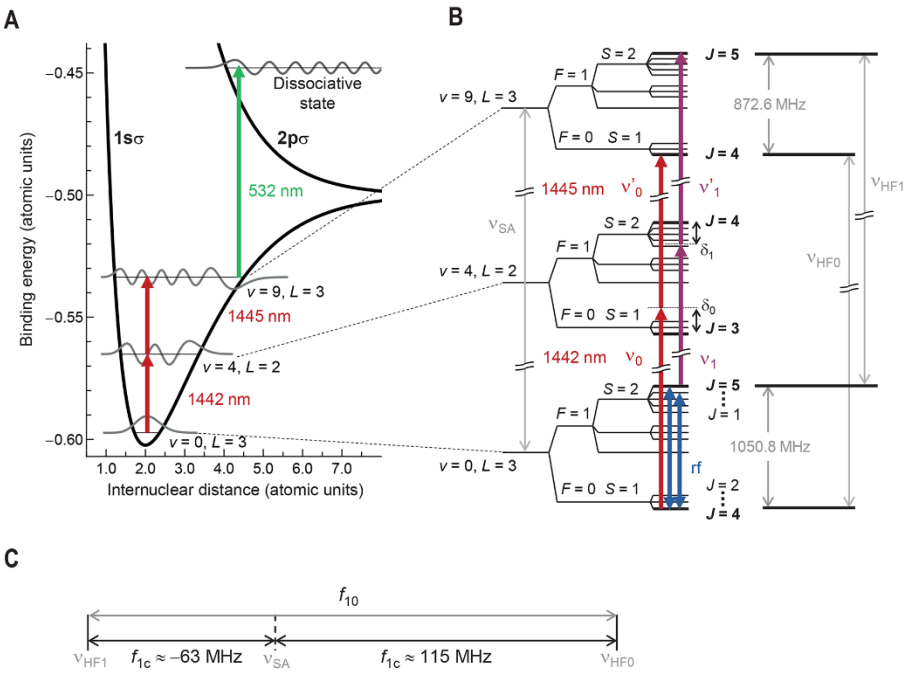

Fig. 1. Partial level diagram and multi-photon transitions. (**A**) Two-photon transitions are driven between rovibrational states with (v,L) = (0,3) and (9,3) in the 1sσ electronic ground state of HD^+. State-selective dissociation of v = 9 population is induced through excitation to the antibonding 2pσ electronic state by a 532 nm photon. (**B**) Spin-averaged transition frequency, ν_{SA}, and hyperfine structure (not to scale) of the levels involved in the two-photon transition, and graphical definitions of the frequencies and detunings of the electromagnetic fields driving transitions between them. (**C**) Graphical definition of the hyperfine intervals in the two-photon transition.

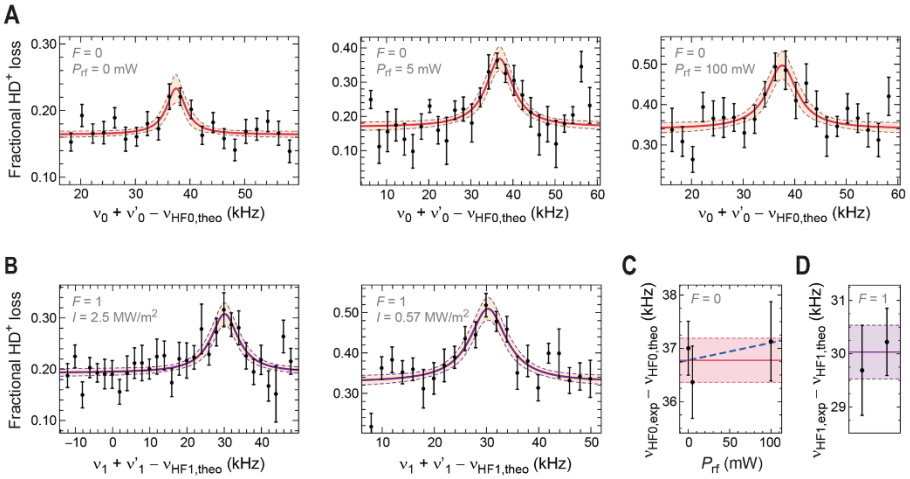

Fig. 2. Spectra of the two-photon transition at 415 THz. (**A**) Spectra of the $F = 0$ transition at various levels of the rf power, P_{rf}. Lorentzian line fits are shown along with 68% confidence-level bands. Each data point represents the mean of a set of typically nine individual measurements, with the error bar indicating the standard error of the mean. (**B**) Spectral data and Lorentzian line fits for the $F = 1$ transitions at two different values of the 532-nm-laser intensity, I. (**C**) Fitted line centers of the $F = 0$ transitions (corrected for systematic shifts (*22*)) shown in (A) are additionally used to check for a possible quasi-resonant ac Zeeman shift by fitting a linear model and extrapolating to 0 mW. The fit (dashed blue line) implies no significant shift. The zero-field $F = 0$ frequency and uncertainty are indicated by the red horizontal line and pink bands, respectively. (**D**) $F = 1$ line-center frequencies from the fits shown in (B), after correction for systematic shifts (*22*). The purple line and bands indicate the weighted mean and uncertainty, respectively.

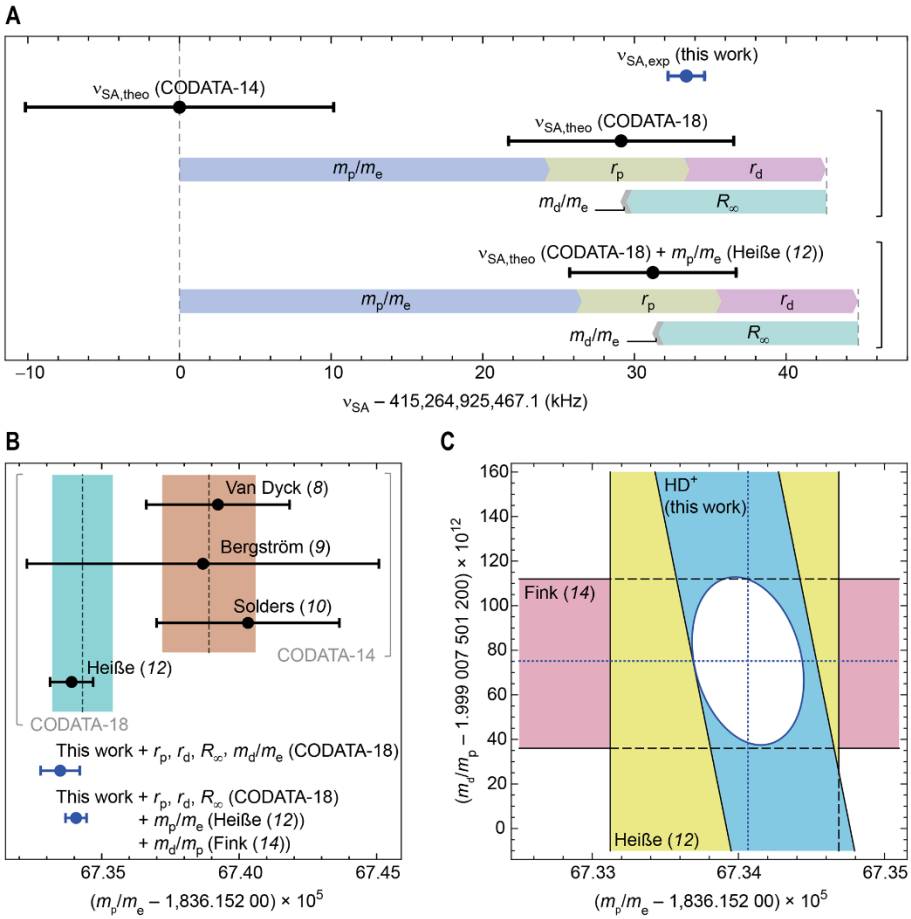

Fig. 3. Implications for the values of physical constants. (**A**) Comparison between $\nu_{SA,exp}$ and theoretical frequencies $\nu_{SA,theo}$ (k) obtained for the indicated combinations of physical constants, k. Arrows represent the cumulative frequency shift introduced by consecutively replacing the CODATA-2014 values of m_p/m_e (blue), r_p (yellow), r_d (red), R_∞ (green), and m_d/m_e (gray), with their counterparts of the set k. (**B**) Values and uncertainties of m_p/m_e from this work (blue data points) compared with measured m_p values from other sources, which were converted to values of m_p/m_e through division by m_e (CODATA-2018). The bottommost blue data point represents the value derived in (C). Dashed lines and shaded areas represent CODATA values and their ±1σ ranges, with brackets indicating which of the measurements shown were included in the respective CODATA adjustments. (**C**) Simultaneous constraint on m_p/m_e and m_d/m_p from HD$^+$ and recent independent measurements of these quantities, leading to new values of m_p/m_e and m_d/m_p, indicated by the blue dotted lines, and the corresponding 1σ-constrained region indicated by the white ellipse.

Table 1. Leading systematic shifts and uncertainties. Shifts and their standard uncertainties (within parentheses) are given in kHz. Their justification can be found in (*22*), as well as the complete error budget (table S2).

Description	$F = 0$ transition	$F = 1$ transition
dc Zeeman effect	0.02(1)	0.10(1)
ac Stark effect 532 nm laser	0.41(10)	0.46(11)
ac Stark effect 1442 nm laser	−0.06(1)	−0.01(0)
ac Stark effect 1445 nm laser	0.03(1)	−0.11(3)
Atomic frequency reference and ultrastable laser drift	−0.02(42)	−0.02(42)
Total systematic shifts	**0.38(43)**	**0.42(43)**
Uncertainty of fitted optical transition frequencies	0.00(41)	0.00(51)
Total systematic shifts + fitted optical frequencies	**0.38(59)**	**0.42(66)**

Table 2. Experimental and theoretical transition frequencies and hyperfine intervals. Uncertainties are given within parentheses, and justified in detail in (*22*). The uncertainties of hyperfine intervals include the expansion factor of about two. During data acquisition and in Fig. 2, theoretical frequency values $\nu_{HF0,theo}$ and $\nu_{HF1,theo}$ based on CODATA-2014 constants were used as offset values; these are included for completeness and labeled with an asterisk. All other theoretical frequency values are obtained using CODATA-2018 physical constants.

Symbol	Value (kHz)
$\nu_{HF0,theo}$*	415,265,040,466.8
$\nu_{HF1,theo}$*	415,264,862,219.1
$\nu_{HF0,exp}$	415,265,040,503.6(0.6)
$\nu_{HF1,exp}$	415,264,862,249.2(0.7)
$f_{0c,theo}$	114,999.7(1.9)
$f_{1c,theo}$	−63,248.0(2.1)
$f_{10,theo}$	178,247.7(3.3)
$f_{10,exp}$	178,254.4(0.9)
$\nu_{SA,theo}$	415,264,925,496.2(7.4)
$\nu_{SA,exp}$	415,264,925,500.5(1.2)

Proton-electron mass ratio from laser spectroscopy of HD^+ at the part-per-trillion level

Sayan Patra, M. Germann, J.-Ph. Karr, M. Haidar, L. Hilico, V. I. Korobov, F. M. J. Cozijn, K. S. E. Eikema, W. Ubachs and J. C. J. Koelemeij

published online July 30, 2020